Void growth in metals: Atomistic calculations

Sirirat Traiviratana [a], Eduardo M. Bringa [b], David J. Benson [a], Marc A. Meyers [a,c,*]

[a] *Department of Mechanical and Aerospace Engineering, University of California, San Diego, La Jolla, CA 92093, USA*
[b] *Materials Science Department, Lawrence Livermore National Laboratory, Livermore, CA 94550, USA*
[c] *NanoEngineering, University of California, San Diego, La Jolla, CA 92093, USA*

Abstract

Molecular dynamics simulations in monocrystalline and bicrystalline copper were carried out with LAMMPS (Large-scale Atomic/ Molecular Massively Parallel Simulator) to reveal void growth mechanisms. The specimens were subjected to tensile uniaxial strains; the results confirm that the emission of (shear) loops is the primary mechanism of void growth. It is observed that many of these shear loops develop along two slip planes (and not one, as previously thought), in a heretofore unidentified mechanism of cooperative growth. The emission of dislocations from voids is the first stage, and their reaction and interaction is the second stage. These loops, forming initially on different {1 1 1} planes, join at the intersection, if the Burgers vector of the dislocations is parallel to the intersection of two {1 1 1} planes: a ⟨1 1 0⟩ direction. Thus, the two dislocations cancel at the intersection and a biplanar shear loop is formed. The expansion of the loops and their cross slip leads to the severely work-hardened region surrounding a growing void. Calculations were carried out on voids with different sizes, and a size dependence of the stress threshold to emit dislocations was obtained by MD, in disagreement with the Gurson model which is scale independent. This disagreement is most marked for the nanometer sized voids. The scale dependence of the stress required to grow voids is interpreted in terms of the decreasing availability of optimally oriented shear planes and increased stress required to nucleate shear loops as the void size is reduced. The growth of voids simulated by MD is compared with the Cocks–Ashby constitutive model and significant agreement is found. The density of geometrically necessary dislocations as a function of void size is calculated based on the emission of shear loops and their outward propagation. Calculations are also carried out for a void at the interface between two grains to simulate polycrystalline response. The dislocation emission pattern is qualitatively similar to microscope observations.
© 2008 Acta Materialia Inc. Published by Elsevier Ltd. All rights reserved.

Keywords: Void growth; Dislocations; Nanocrystalline materials; Copper; Molecular dynamics simulations

1. Introduction

Fracture of ductile metals occurs by nucleation, growth and coalescence of voids [1]. There have been a number of continuum models proposed for the growth of voids in both two and three dimensions [2–5]. However, until recently there was no well established atomistic mechanism for void growth, and the model proposed by Cuitiño and Ortiz [6] is based on vacancy pipe diffusion. The only exception is Stevens et al. [7], who proposed a dislocation model for void growth in spalling.

Lubarda et al. [8] demonstrated that the vacancy diffusion mechanism is only applicable at low strain rates and/ or high temperatures, and is therefore only relevant in creep deformation. Indeed, failure in creep is preceded by void nucleation and growth at the grain boundaries, and has been successfully modeled using the diffusion equation by Raj and Ashby [9]. Under these conditions vacancies definitely play a key role. The strain rates encountered in conventional deformation are on the order of 10^{-3} s^{-1}; in laser shock the strain rates are on the order of 10^6 s^{-1} and higher. Hence, one cannot envisage a vacancy diffusion mechanism under most operating conditions.

Analytical results by Lubarda et al. [8] and molecular dynamics simulations by Rudd and co-workers [10–13]

* Corresponding author. Tel.: +1 858 534 4719.
 E-mail address: mameyers@ucsd.edu (M.A. Meyers).

and Marian et al. [14,15] indicate that dislocation emission from the growing voids is the primary mechanism of radial material transfer required for void expansion. Void collapse calculations [16,17] lead to similar (but opposite in sign) dislocation configurations. Both prismatic and shear loops were postulated [8] and observed in molecular dynamics (MD) simulations [10–15,18]. Potirniche et al. [19] studied the expansion of voids with radii varying between 0.75 and 4.5 nm in monocrystalline nickel using a modified embedded atom method. Fig. 1 shows the two types of dislocation loops. It should be noted that Ashby [20–22] had also postulated prismatic and shear loops in the deformation of metals containing rigid particles to accommodate the strain gradients imposed; these are the "geometrically necessary dislocations". Seitz [23] and Brown [24] postulated prismatic loops forming at the interface between rigid article and the matrix. Thus, the suggestion that void growth takes place by shear and prismatic loop expansion is well rooted in inhomogeneous plastic deformation. It is the objective of this report to analyze the growth of voids in greater detail. The grain-boundary nature and void size were altered to examine their effect on growth mechanisms.
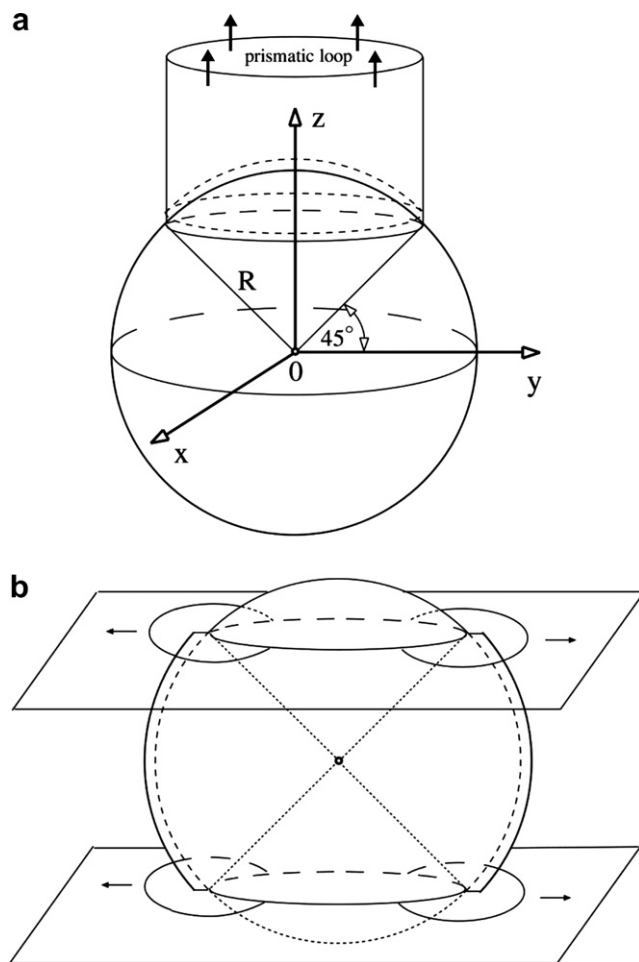

Fig. 1. Dislocation loops postulated by Lubarda et al. [8]; direction of dislocation motion marked by arrows. (a) Prismatic loops and (b) shear loops.

Atomistic simulation performed by Horstemeyer et al. [25] in simple shear using between 10^2 and 10^8 atoms revealed significant differences in the flow stress when expressed as a function of a scale parameter (volume/surface of sample). The resolved shear stress for plastic flow increases significantly with the decrease in size-scale, confirming experimental measurements related to gradient plasticity effects (e.g., Fleck et al. [33,34]). Interestingly, the MD results indicate that dislocation nucleation effects and not strain gradient effects (calculations in simple shear do not produce strain gradients) are responsible for the significant differences in shear flow stress obtained with the change in dimensional scale. These results have a significant bearing in what is perceived to be gradient plasticity.

2. Experimental observation

Dislocation activity around a void growing in the spall regime of shock compressed copper was reported by Meyers and Aimone [26] and Christy et al. [27]. There are also reports in the literature of a work-hardened layer surrounding a growing void (e.g. Ahn et al. [18]). Fig. 2 shows slip bands emanating from voids that nucleated at grain boundaries in copper. It is clear that void expansion did not occur by vacancy migration or prismatic loop emission, since slip bands, emanating from the void surface, are clearly seen. However, the exact nature of dislocation generation and evolution cannot be obtained from these observations. This requires detailed analysis methods such as MD.

3. Computational approach

The molecular dynamics LAMMPS (Large-scale Atomic/Molecular Massively Parallel Simulator) [28] code was used in this investigation. For the face-centered cubic copper structure, an EAM [29] Mishin et al. [30] potential was used. The number of atoms was varied from 10^5 to 10^7, and calculations were performed on parallel PCs and on the supercomputer at San Diego super computer center.

The single crystal copper domain was $10 \times 10 \times 10$ nm with 1 nm radius spherical void at center. This gives a void volume fraction of 0.42%. A periodic boundary was used with uniaxial expansion strain. The domain size was reduced for 0.5 nm radius void and enlarged for 2.0 nm radius void while fixing void volume fraction at 0.42%. The different sized domains were subjected to uniaxial strain along [0 0 1]. All simulations were done at a strain rate of 10^8 s^{-1} (2000 ps, 20% volume strain). Visualization of stacking faults representing dislocations was done with a filter using a centrosymmetry parameter [31].

A bicrystal copper domain was constructed with two single crystal cubes sharing a tilt boundary making an angle, $\theta = 43.6°$. The random angle of 43.6° between two grains (1, left and 2, right) was chosen because it rotates the atoms into positions that produce simple indices in LAMMPS. A counterclockwise rotation around [1 0 0] of
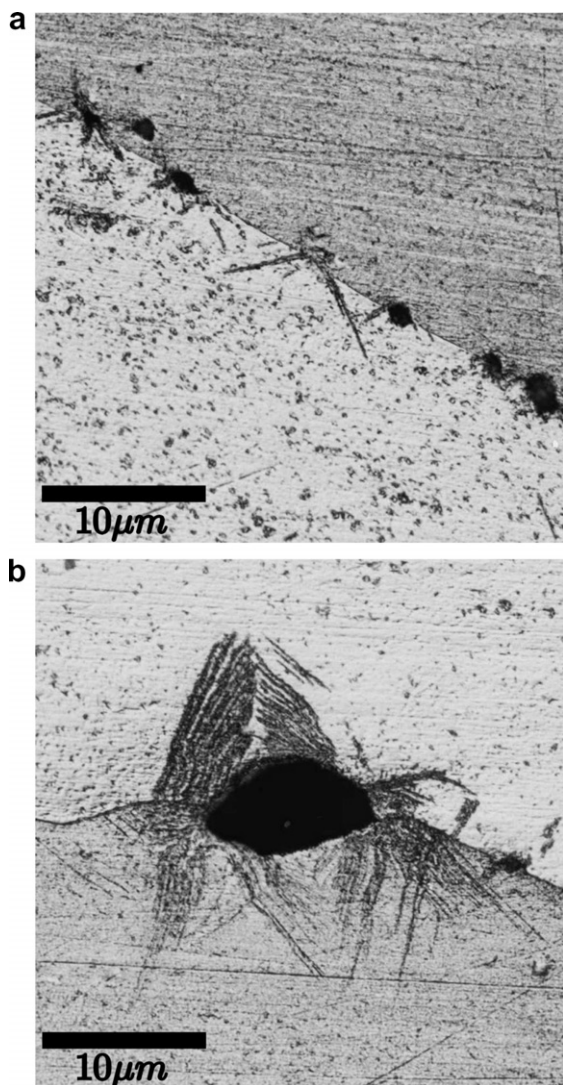
Fig. 2. Evidence of slip around growing grain-boundary voids: (a) Small voids and (b) large void.

21.8° for grain 1 and of 21.8° (clockwise) for grain 2 were taken. This rotation transformed the directions $[0\,1\,0]$ and $[0\,0\,1]$ from the original referential into ones with reasonably small indices: $[0\,5\,\bar{2}]$ and $[0\,2\,5]$ for grain 1 and $[0\,5\,2]$ and $[0\,\bar{2}\,5]$ for grain 2, respectively. The domain underwent annealing and relaxation to minimize grain-boundary energy; a spherical void was cut followed by a second relaxation to minimize void surface energy. Uniaxial volume strain was applied at a strain rate of $5 \times 10^9\,\text{s}^{-1}$; the void radius was 18 nm.

4. Results

4.1. Void size dependence of critical stress

A size-scale dependence of yield stress can be observed in uniaxial strain simulations with various sizes of domains (Fig. 3). The void fraction was kept constant at 0.42%. As the void size increases, the yield stress drops: it is 11 GPa
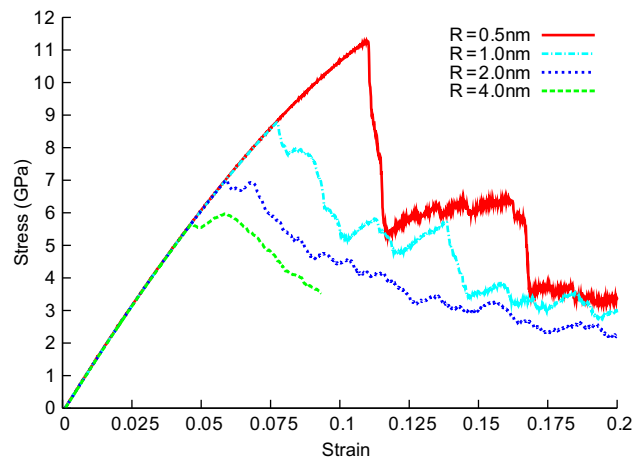

Fig. 3. Stress–strain relations for different void sizes, showing size-scale dependence of yield stress.

for 0.5 nm and 7 GPa for 2 nm void. It should be mentioned that Potirniche et al. [19] have made similar calculations for nickel. Their void radius was varied from 0.75 to 4.5 nm whereas in the current calculations they were varied from 0.5 to 2 nm. Potirniche et al. [19] used a constant ratio of specimen to void dimensions. Other differences with the current calculations are the lateral boundary conditions; the boundaries were assumed free by Potirniche et al. [19] whereas the state was assumed to be uniaxial strain with periodic boundary conditions. There is also a significant difference in strain rate: Potirniche et al. [19] used $10^{10}\,\text{s}^{-1}$, whereas we used $10^8\,\text{s}^{-1}$. This lower strain rate enabled individual observation of dislocations. In spite of the differences, the stresses calculated herein are in good agreement with the ones by Potirniche et al. [19] for nickel; the ratios of stress to shear modulus vary from 0.12 to 0.22 in our calculations and from 0.17 to 0.26 in Fig. 8 of Potirniche et al. [19].

The void size dependence is in opposition to the Gurson criterion [2], which is size independent: $\sigma_y = g(f, \sigma_{kk}, \sigma_e)$. The stress at which the quasi-linear behavior is no longer obeyed is taken as the yield stress; it corresponds to the onset of dislocation activity. The stress drop is substantial for the smallest void radius (0.5 nm); this is due to the fact that domain size is the smallest. For the larger voids, a greater extent of dislocation interaction takes place before the dislocations reach the boundaries of the "box". It is interesting that these results can also be interpreted in the framework of gradient plasticity [32–38]. However, this transcends the goal of this report.

Fig. 4a shows the yield stress (normalized to the shear modulus, G) plotted as a function of the normalized void radius, R/b, where b is the Burgers vector. The decrease of yield stress with increasing R/b is clear, similar to Dávila et al. [16]. The von Mises stress was obtained from the three components of the principal stress in the uniaxial strain state. The atomistic results compare well with the analytical calculations by Lubarda et al. [8], which are obtained from
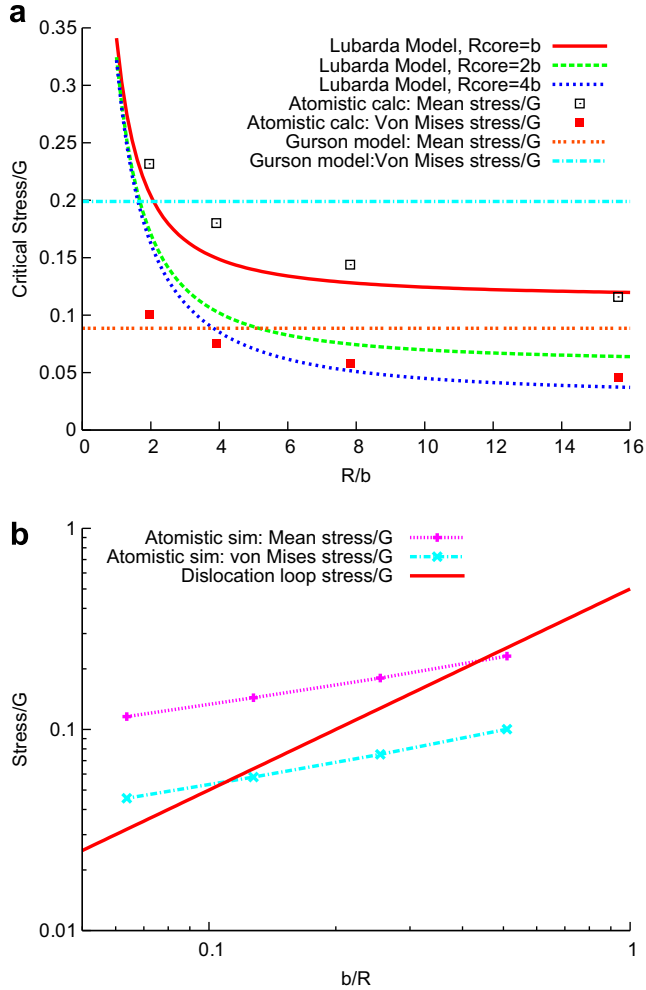
Fig. 4. Normalized critical stress against normalized void size: (a) with models and (b) on log–log scale.

The condition for plastic flow is

$$\Phi = 0 \tag{5}$$

The decomposition of strain into hydrostatic and deviatoric parts is

$$\varepsilon = \begin{bmatrix} \varepsilon_x & 0 & 0 \\ 0 & 0 & 0 \\ 0 & 0 & 0 \end{bmatrix} = \begin{bmatrix} \frac{1}{3}\varepsilon_x & 0 & 0 \\ 0 & \frac{1}{3}\varepsilon_x & 0 \\ 0 & 0 & \frac{1}{3}\varepsilon_x \end{bmatrix} + \begin{bmatrix} \frac{2}{3}\varepsilon_x & 0 & 0 \\ 0 & -\frac{1}{3}\varepsilon_x & 0 \\ 0 & 0 & -\frac{1}{3}\varepsilon_x \end{bmatrix} \tag{6}$$

The corresponding stresses are

$$\boldsymbol{\sigma} = \sigma_{\text{hydrostatic}} + \sigma_{\text{deviatoric}}$$

$$= K \begin{bmatrix} \frac{1}{3}\varepsilon_x & 0 & 0 \\ 0 & \frac{1}{3}\varepsilon_x & 0 \\ 0 & 0 & \frac{1}{3}\varepsilon_x \end{bmatrix} + 2G \begin{bmatrix} \frac{2}{3}\varepsilon_x & 0 & 0 \\ 0 & -\frac{1}{3}\varepsilon_x & 0 \\ 0 & 0 & -\frac{1}{3}\varepsilon_x \end{bmatrix} \tag{7}$$

where K is bulk modulus and G is shear modulus. From Eq. 4

$$\sigma_h = K\varepsilon_x \tag{8}$$

with deviatoric stress from Eqs. 3 and 7

$$\sigma_e^2 = 4G^2\varepsilon_x^2 \tag{9}$$

The Gurson yield function now becomes

$$\Phi = \frac{4G^2\varepsilon_x^2}{\sigma_y^2} + 2f \cosh\left(\frac{K\varepsilon_x}{2\sigma_y}\right) - 1 - f^2 \tag{10}$$

We can assume, to a first approximation, that strain rate imparted to the material ($10^8\,\text{s}^{-1}$) is such that the theoretical shear stress is reached. Thus

$$\tau = \frac{\sigma_y}{2} \simeq \frac{G}{10} \tag{11}$$

G is 48.7 GPa, K is 130 GPa and σ_y is 9.74 GPa. With $f = 0.0042$, one obtains $\varepsilon_x = 0.099484$, which results in a von Mises stress of 9.6897 GPa and a mean stress of 4.311 GPa. These values are introduced into Fig. 4a for comparison purposes. It can be seen that the Gurson model [2] is in reasonable agreement with the analytical Lubarda et al. [8] results and the MD calculations for larger void sizes. However, it does not have a void size dependence. Wen et al. [39] modified Gurson's model by incorporating the Taylor dislocation model. With the introduction of this scale dependent hardening component, the stress required to expand voids became scale dependent. This corresponds to the incorporation of gradient plasticity [32–38] into Gurson's model.

It is instructive to establish whether the void size dependence of the flow stress is directly linked to the stress required to bow dislocation loops into semi-circles (the stress minimum). Thus, the expression, e.g. [40], was used

$$\frac{\sigma}{G} = \alpha \frac{b}{R} \tag{12}$$

where α is a parameter equal to approximately 0.5 and R was taken as the void radius (assuming that loop and void

$$\frac{\sigma_{cr}}{G} = \frac{b/R}{\sqrt{2}\pi(1-v)} \frac{(1 + \sqrt{2}R_{core}/R)^4 + 1}{(1 + \sqrt{2}R_{core}/R)^4 - 1} \tag{1}$$

where the radius of the core, R_{core}, was made equal to b, $2b$ and $4b$. The stresses calculated by Lubarda et al. [8] are local values at the surface of the void, whereas the current values are from the far field, and therefore a correction factor of 2 (stress concentration for the spherical void) was introduced.

By contrast, Gurson's formulation [2] is void size independent, since only the porosity, f, enters the expression:

$$\Phi = \frac{\sigma_e^2}{\sigma_y^2} + 2f \cosh\left(\frac{\sigma_h}{2\sigma_y}\right) - 1 - f^2 \tag{2}$$

where σ_y is the uniaxial yield stress of the material, σ_e is the equivalent von Mises stress and σ_h is the hydrostatic stress. The latter two are

$$\sigma_e = \left[\frac{3}{2}\sigma'_{ij}\sigma'_{ij}\right]^{\frac{1}{2}} \tag{3}$$

$$\sigma_h = \sigma_{kk} \tag{4}$$

radii are the same, to a first approximation). The results are plotted in Fig. 4b. In the log–log scale, both stresses obtained from atomistic simulations are linear and have expressions

$$\frac{\sigma_m}{G} = 0.2884 \left(\frac{b}{R}\right)^{0.3323}$$
$$\frac{\sigma_e}{G} = 0.1288 \left(\frac{b}{R}\right)^{0.3798} \quad (13)$$

The exponents and pre-exponential factors in the atomistic calculation are 0.33–0.38 and 0.13–0.29, in contrast with Eq. (12), in which they are 1 and 0.5, respectively. Nevertheless, the compatibility of the results is strong evidence that loop expansion beyond a semi-circle is an important contributing mechanism.

4.2. Two-dimensional dislocation reactions

For the shear loops postulated by Lubarda et al. [8] to undergo continued expansion, they have to intersect if they form in the same (1 1 1). Six loops with edge dislocations at the center create the uniform expansion of the void segment (calota) if they can expand uniformly. In this section the energetics of the process are analyzed. Fig. 5 shows three dislocations ($[0\bar{1}1]$, $[\bar{1}01]$ and $[\bar{1}10]$) in the (1 1 1) plane that intersects the void at 45°. These are the planes (shown in Fig. 1b) that maximize the shear stress. Three nascent loops are shown in Fig. 5a; as they expand

(Fig. 5b), their extremities touch and this would encourage a reaction. We analyze this for perfect and partial dislocations in Sections 4.2.1 and 4.2.2, respectively.

4.2.1. Perfect in-plane dislocation loops

Fig. 5b shows three dislocation loops with Burgers vectors $\vec{b}_1, \vec{b}_2$ and $\vec{b}_3$. The resulting reaction will lead to (Fig. 5c):

$$\vec{b}_1 + \vec{b}_2 = \vec{b}_7 \quad (14)$$

The Burgers vector of $\vec{b}_7$ is (the Burgers vectors have to be subtracted in order to account for the dislocation lines; this is analogous to the interaction in a Frank–Read source):

$$\frac{a}{2}[\bar{1}01] + (-)\frac{a}{2}[\bar{1}10] = \frac{a}{2}[0\bar{1}1] \quad (15)$$

The simple energy reduction criterion is obeyed $\left(E = G\frac{b^2}{2}\right)$ and the reaction takes place

$$G\frac{a^2}{2} + G\frac{a^2}{2} > G\frac{a^2}{2} \quad (16)$$

Additionally, there is a change in overall dislocation length when reaction occurs as shown in Fig. 5c. One can estimate the equilibrium of the dislocation configuration by using the energy equation incorporating the lengths.

Thus, the configuration seen in Fig. 5d can be envisaged: six dislocation loops expanding uniformly in the same
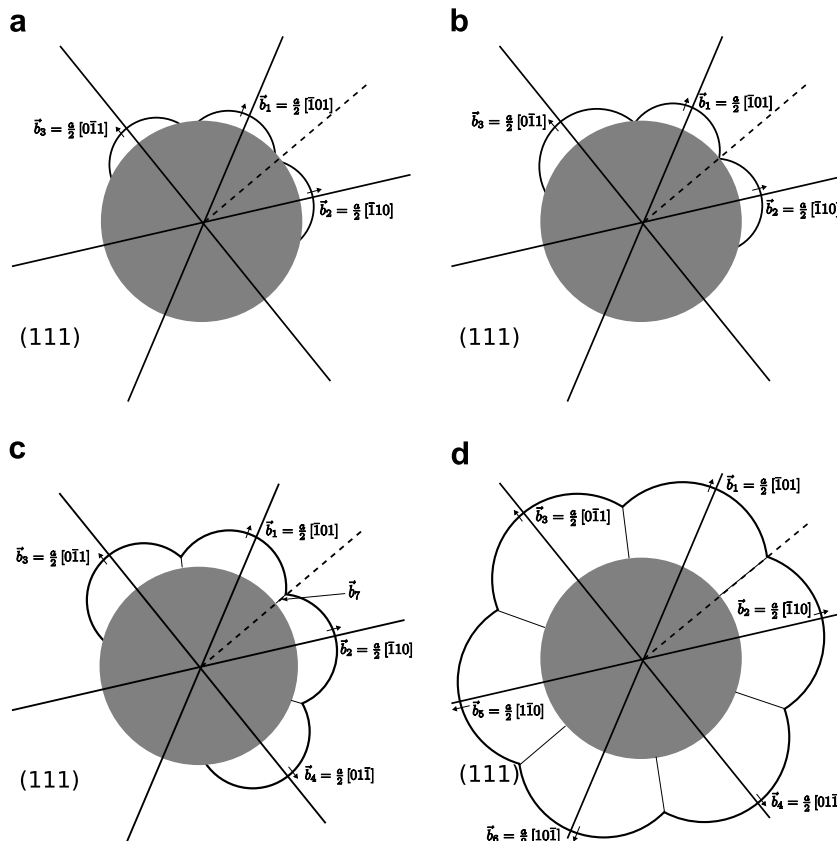

Fig. 5. In-plane dislocation interactions: (a) before interaction; (b) onset of interaction; (c) interactions and reaction and (d) uniform expansion of loops leaving dislocation segments behind.
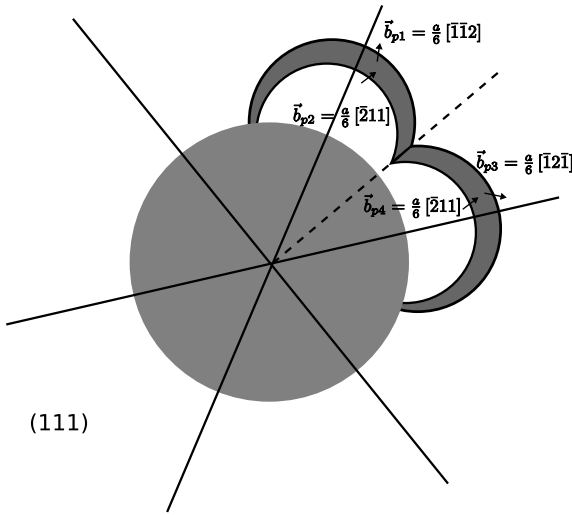
Fig. 6. In-plane partial dislocation interaction.

(1 1 1) plane, creating six segments through reactions. These segments are not mobile but are not sessile, since they have Burgers vectors in (1 1 1). They have edge character, with the Burgers vector perpendicular to the line. This configuration is slightly different from the one described by Marian et al. [14,15].

4.2.2. Partial in-plane dislocation loops

The partial dislocations corresponding to $\vec{b}_1$ in plane (1 1 1) are (Fig. 6)

$$\vec{b}_1 = \frac{a}{2}[\bar{1}\,0\,1] \Rightarrow \vec{b}_{p1} = \frac{a}{6}[\bar{1}\,\bar{1}\,2]; \quad \vec{b}_{p2} = \frac{a}{6}[\bar{2}\,1\,1] \tag{17}$$

The partial dislocations corresponding to $\vec{b}_2$ in plane (1 1 1) are

$$\vec{b}_2 = \frac{a}{2}[\bar{1}\,1\,0] \Rightarrow \vec{b}_{p3} = \frac{a}{6}[\bar{1}\,2\,\bar{1}]; \quad \vec{b}_{p4} = \frac{a}{6}[\bar{2}\,1\,1] \tag{18}$$

The leading partials react as (again, we have to subtract $\vec{b}_{p3}$ from $\vec{b}_{p1}$ to account for dislocation line direction normalization)

$$\vec{b}_{p1} + \vec{b}_{p3} = \frac{a}{6}[\bar{1}\,\bar{1}\,2] + (-)\frac{a}{6}[\bar{1}\,2\,\bar{1}] = \frac{a}{2}[0\,\bar{1}\,1] \tag{19}$$

The trailing reaction produces

$$\vec{b}_{p2} + \vec{b}_{p4} = \frac{a}{6}[\bar{2}\,1\,1] + (-)\frac{a}{6}[\bar{2}\,1\,1] = 0 \tag{20}$$

This is the same solution as for perfect dislocations, as expected. It is interesting to note that the leading partials react, creating a perfect dislocation and the trailing partials cancel.
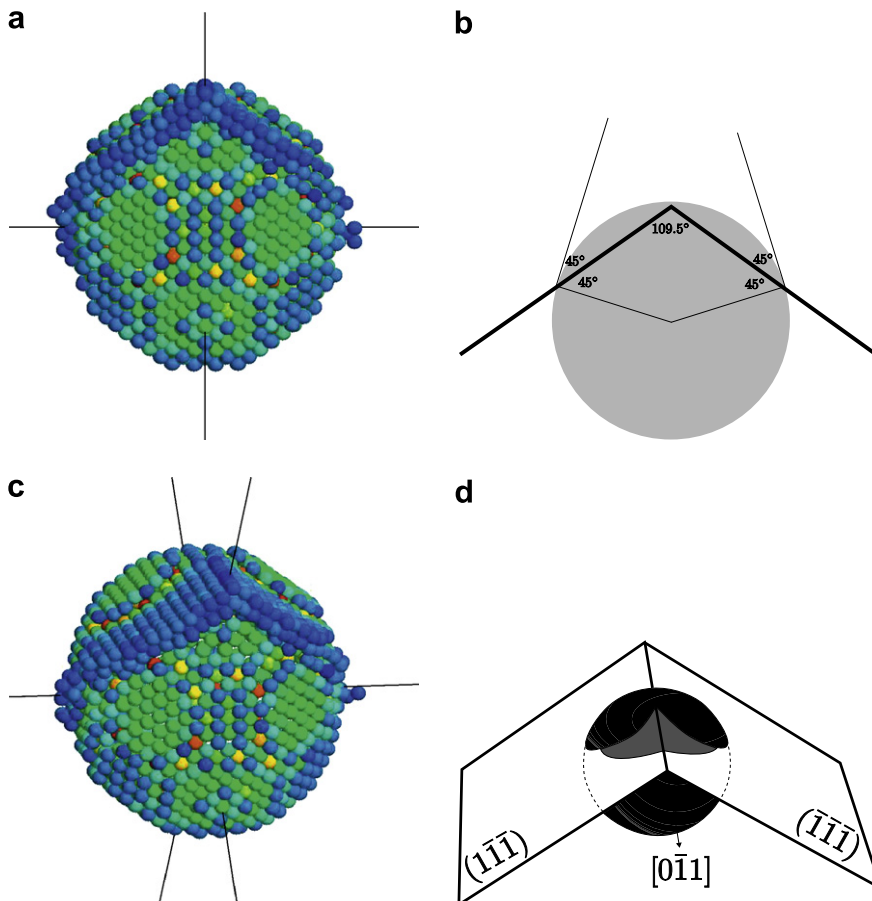

Fig. 7. Initiation of plastic flow at void surface (at 590 ps): (a) rendered atoms from MD; (b) diagram of $(1\bar{1}\bar{1})$ and $(\bar{1}\bar{1}\bar{1})$ slip planes intersecting sphere surface at 45°; (c) rendered atoms from (a), rotated to show two loops and (d) diagram showing leading partial dislocations.

4.3. Atomistic simulation of dislocation activity

Figs. 7 and 8 shows both the MD simulations (left) and models (right) for initiation and propagation of dislocations. Shear loops on different {1 1 1} planes, making 45° with the void, connect at the ⟨1 1 0⟩ intersection (Fig. 7b). Fig. 7a and c shows two views of a biplanar dislocation loop starting to form. This is more clear in the schematic of Fig. 7d, which shows the leading partials fully formed. As the leading partials expand, the trailing partials follow them. More complex dislocation interactions take place as the shear loops propagate outwards (Fig. 9).

In general, the stacking fault consists of two layers of atoms composing the plane of the dislocation. Fig. 8 shows the continued expansion of the biplanar loops. When an additional layer forms on top of these two layers, the plane opens up with trailing edge of dislocation closing the stacking fault. At this point, it becomes a shear loop with a narrow stacking fault band. Shear loops continue to travel outwards from the void surface as they transport material, accommodating the growth of void.

Bicrystal simulation, although done at much higher strain rate (5×10^9 s^{-1}) shows results consistent with single crystal void growth. Partial dislocation loops are emitted from the void surface, interact and travel together as the strain increases (Fig. 10). One can see at least two biplanar shear loops emanating from the void in Fig. 10 (marked

1 and 2), one in each grain. The dislocation interactions are more complex because the number of slip planes involved is twice as high. Figs. 11 and 12 show the two-dimensional sections perpendicular to the grain-boundary (left) and three-dimensional views (right) at different times (40–45 ps). The evolution of shear is evident, and the similarity with the experimental observations of Fig. 2 is striking. Slip emanates from the void starting in Fig. 11c and propagates outward along ⟨1 1 1⟩; shear loops are activated in the two grains shown in Fig. 12a–c. In Fig. 12c, one can see that the trailing partial follows the leading partial. This can be seen better in the tridimensional views shown in Fig. 12d and f.

The separation of partials in MD calculations has been the object of considerable study, and the potential used influences these values. Van Swygenhoven et al. [41] discuss this for nanocrystalline metals and point out the importance of two stacking-fault energies (SFEs): the stable and the unstable one. The generalized planar fault energy curve provides the barrier that the leading and trailing partial dislocations encounter. This barrier has two cusps with a trough between them. The first cusp corresponds to the unsteady SFE and the second cusp to the steady SFE. Van Swygenhoven et al. [41] warn the readers of the limitations of the MD analysis, where both the high stresses and short timescales can affect the separation between partials. Table 1 shows the stable and unstable SFEs for different potentials used. There is some variation. The nucleation
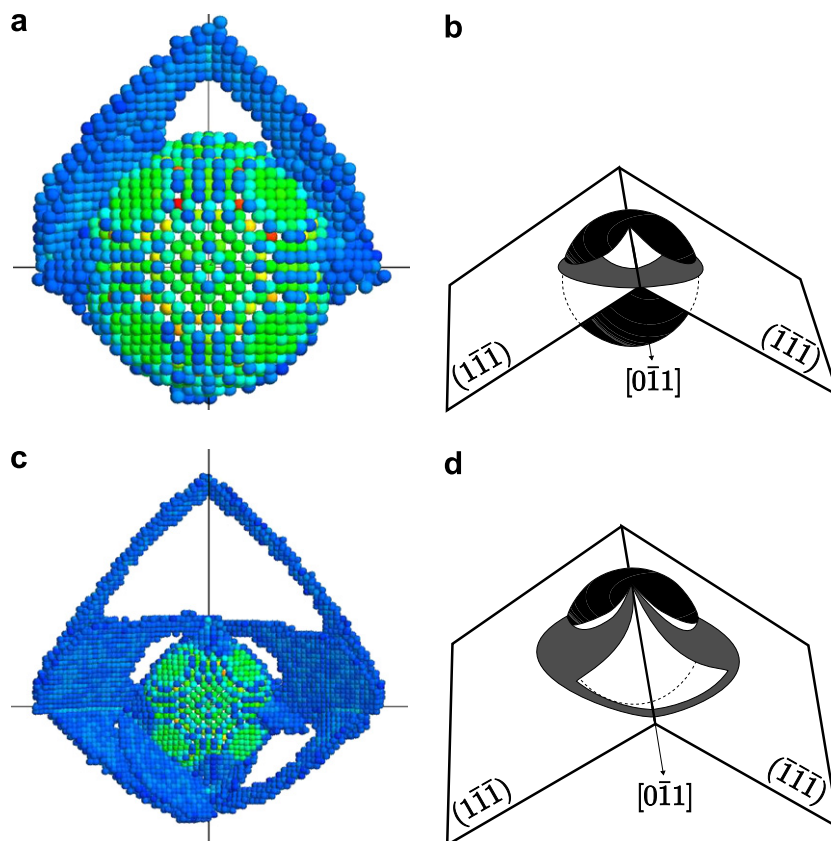

Fig. 8. Continued loop expansion: (a) rendered atoms from MD (591 ps); (b) corresponding sketched diagram; (c) rendered atoms from MD (595 ps) and (d) corresponding sketched diagram.
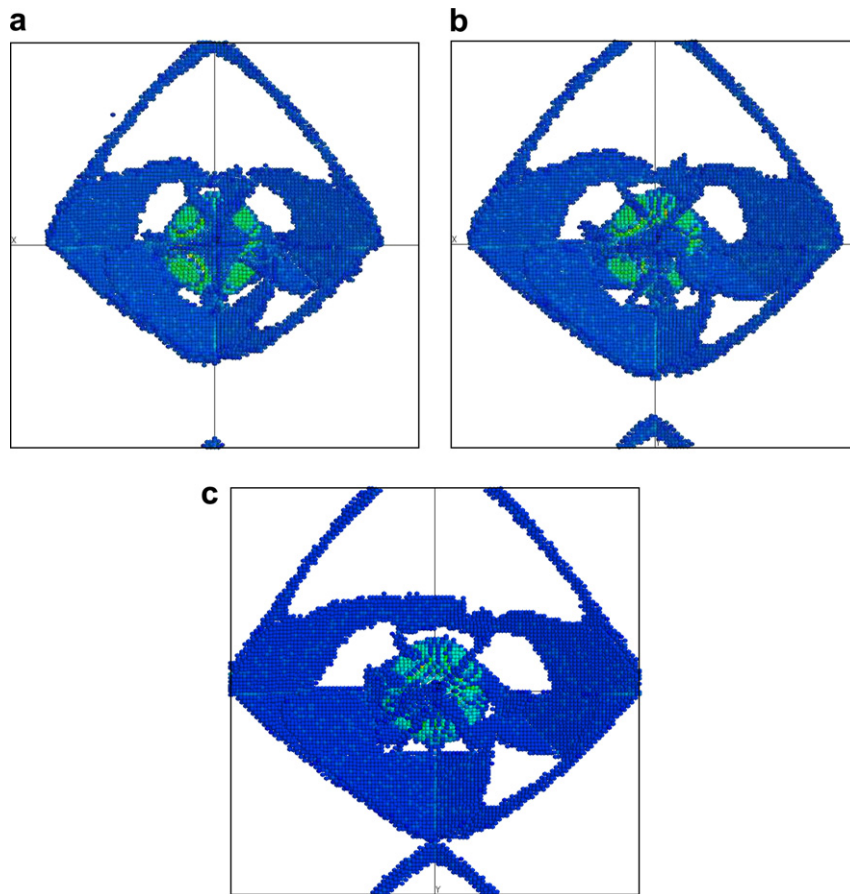
Fig. 9. Later growth and interaction of shear loops emanating from void: (a) 597 ps; (b) 598 ps and (c) 599 ps.
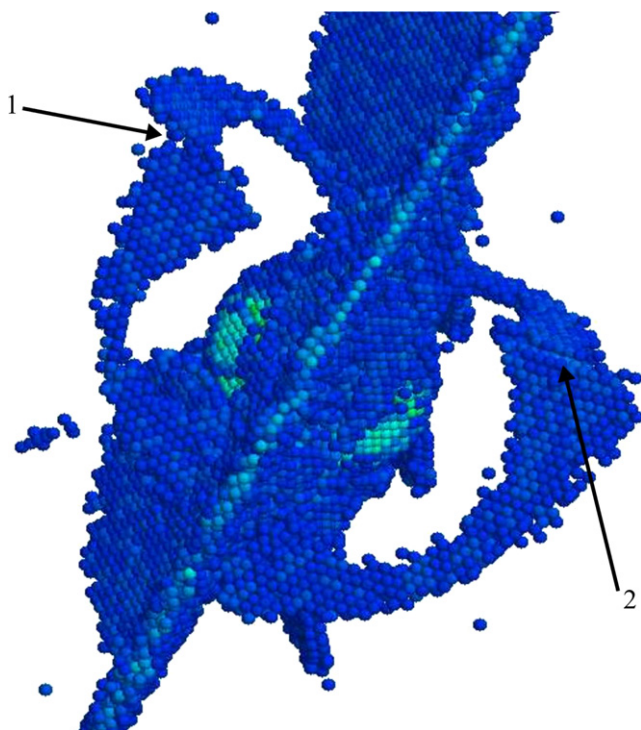

Fig. 10. Shear loops and their interaction in bicrystal simulation with initial void at grain-boundary (uniaxial strain).

of the trailing dislocation encounters the energetic barrier $(\gamma_{USF} - \gamma_{SF})$. Hence, we are aware of the limitations of MD in predicting the actual partial separation. Nevertheless, we observe both partials and perfect dislocations and the minimum partial separation observed (Fig. 10) is $(3–5)b$. However, the stacking fault can be considerably larger prior to the nucleation of the trailing partial.

The simulations were carried out under uniaxial strain, not uniaxial stress, as in Potirniche et al. [19]. The lateral stresses have been computed as a function of time and are shown in Fig. 13. The difference between the longitudinal (S_{zz}) and lateral stresses (S_{xx} and S_{yy}) rises linearly until the maximum. At this point, the longitudinal stress decreases as a result of dislocation loop nucleation at the surface of void. There is a modest rise in the transverse stresses. As a result, the three stresses approach each other and the state of stress approaches a hydrostat. As the three stresses decay on unloading, their magnitudes are very close. Hence, the emission of dislocations at the void surfaces relaxes the deviatoric stresses.

4.4. Analysis of biplanar shear loops

A more detailed dislocation representation is shown in Fig. 14a and b (perfect dislocations and partial disloca-
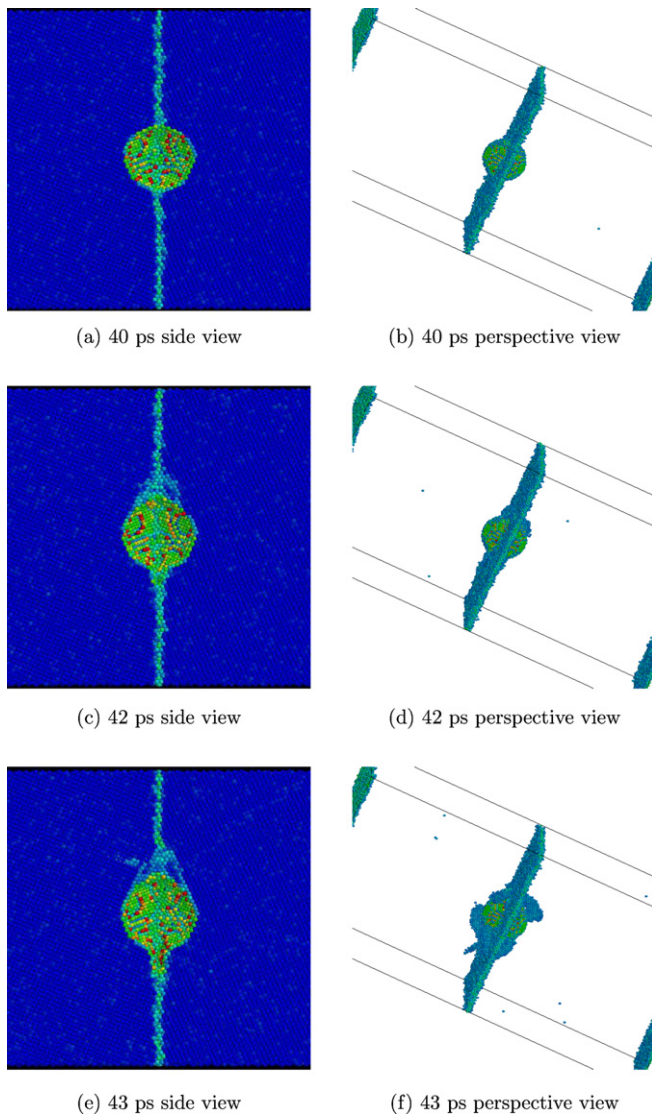
Fig. 11. Sequence of loop nucleation and growth in bicrystal simulation (times: 40–43 ps).
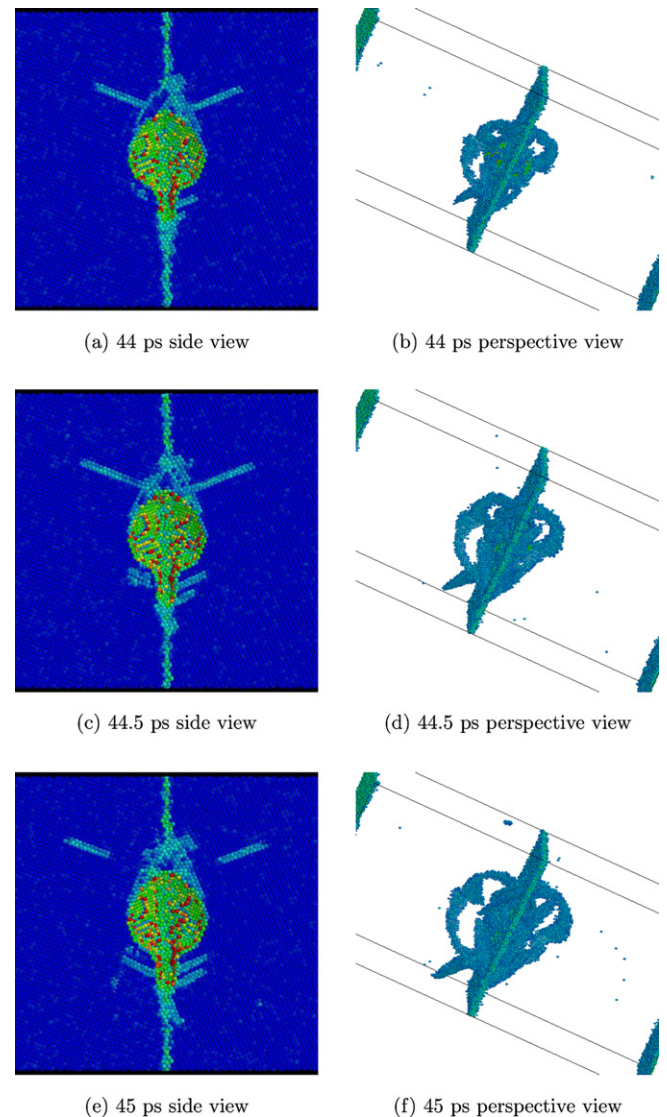

Fig. 12. Sequence of loop nucleation and growth in bicrystal simulation (times: 44–45 ps).

tions, respectively). In Fig. 14a, two perfect dislocation loops, $\vec{b}_1$ and $\vec{b}_2$, forming on $(1\bar{1}\bar{1})$ and $(\bar{1}\bar{1}\bar{1})$, respectively, interact from the early state of dislocation formation. They have parallel Burgers vectors but are on different planes. The intersection line is also aligned with $[0\bar{1}1]$, which allows the two dislocations to glide without forming sessile segments. Actually, they cancel each other at the $\langle 110 \rangle$ intersection. An analysis analogous to the one made in Sections 4.2.1 and 4.2.2 was carried out with the difference that we now use $(1\bar{1}\bar{1})$ and $(\bar{1}\bar{1}\bar{1})$.

4.4.1. Perfect dislocation biplanar interaction

$$\vec{b}_1 + \vec{b}_2 = \vec{b}_7 \qquad (21)$$

$$\frac{a}{2}[0\bar{1}1] + (-)\frac{a}{2}[0\bar{1}1] = 0 \qquad (22)$$

The energy becomes zero at the intersection line, because the two perfect dislocations cancel each other. Thus, the

Table 1
Table of different potentials used for copper

Potential	Reference	γ_{SF} (mJ/m^2)	γ_{USF} (mJ/m^2)
Cleri–Rosato	[42]	20.6	154.1
Schiøtz–Jacobsen	[43]	33.5	173.1
Mishin et al. 1	[30]	44.4	158
Mishin et al. 2	[30]	36.2	161

biplanar loop does not require the creation of a radial dislocation. This is an energetic advantage over the planar loop emission mechanism.

4.4.2. Partial dislocation biplanar interaction

The interaction of perfect dislocations can be extended to partial dislocations (Fig. 14b). The decomposition of a perfect dislocation $\vec{b}_1$ in $(1\bar{1}\bar{1})$ leads to
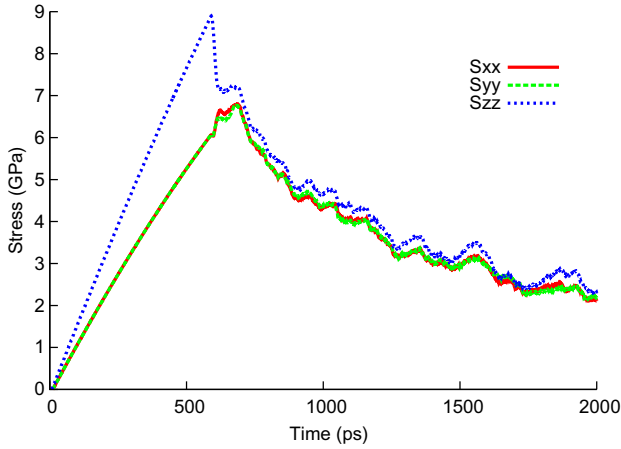
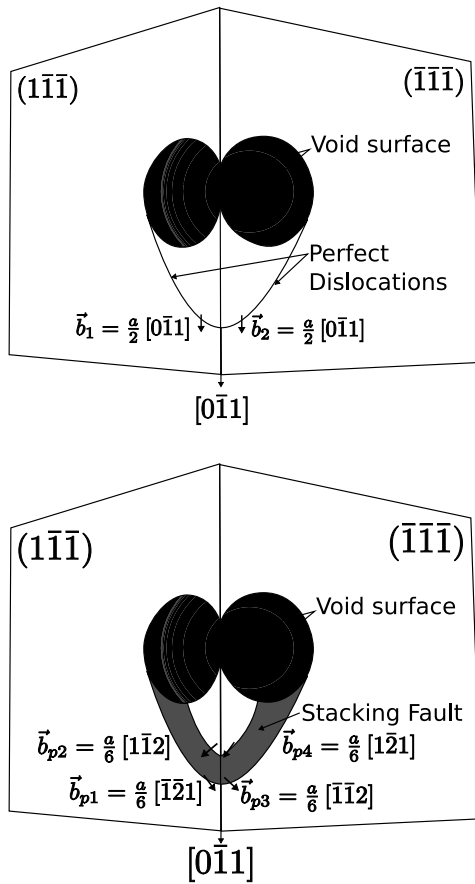Fig. 13. Lateral stresses generated when loading is applied in direction ZZ.

Fig. 14. Top view of loop interaction of biplanar dislocation loops on $(1\bar{1}\bar{1})$ and $(\bar{1}\bar{1}\bar{1})$: (a) perfect dislocations and (b) partial dislocations.

$$\vec{b}_1 = \frac{a}{2}[0\,\bar{1}\,1] \Rightarrow \vec{b}_{p1} = \frac{a}{6}[\bar{1}\,\bar{2}\,1]; \quad \vec{b}_{p2} = \frac{a}{6}[1\,\bar{1}\,2] \tag{23}$$

The energy criterion is ($\propto b^2$)

$$\frac{a^2}{2} > \frac{a^2}{6} + \frac{a^2}{6} = \frac{a^2}{3} \tag{24}$$

The decomposition of a perfect dislocation $\vec{b}_2$ in $(\bar{1}\,\bar{1}\,\bar{1})$ is

$$\vec{b}_2 = \frac{a}{2}[0\,\bar{1}\,1] \Rightarrow \vec{b}_{p3} = \frac{a}{6}[\bar{1}\,\bar{1}\,2]; \quad \vec{b}_{p4} = \frac{a}{6}[1\,\bar{2}\,1] \tag{25}$$

The energy criterion is ($\propto b^2$)

$$\frac{a^2}{2} > \frac{a^2}{6} + \frac{a^2}{6} = \frac{a^2}{3} \tag{26}$$

The reaction between the leading partials is (note the sign change required for normalization of the dislocation line direction)

$$\vec{b}_{p1} + \vec{b}_{p3} : \frac{a}{6}[\bar{1}\,\bar{2}\,1] + (-)\frac{a}{6}[\bar{1}\,\bar{1}\,2] = \frac{a}{6}[0\,\bar{1}\,\bar{1}] \tag{27}$$

The energy criterion is ($\propto b^2$)

$$\frac{a^2}{6} + \frac{a^2}{6} = \frac{a^2}{3} > \frac{a^2}{18} \tag{28}$$

This reaction reduces energy. For the trailing partials

$$\vec{b}_{p2} + \vec{b}_{p4} : \frac{a}{6}[1\,\bar{1}\,2] + (-)\frac{a}{6}[1\,\bar{2}\,1] = \frac{a}{6}[0\,1\,1] \tag{29}$$

The energy criterion is ($\propto b^2$)

$$\frac{a^2}{6} + \frac{a^2}{6} = \frac{a^2}{3} > \frac{a^2}{18} \tag{30}$$

This reaction also reduces energy. The sum of the two reaction products is, as expected, zero. This is consistent with the calculations conducted on biplanar perfect dislocations. Thus the leading partials create a Lomer–Cottrell sessile dislocation $\frac{a}{6}[0\,\bar{1}\,\bar{1}]$; the trailing partials react similarly and create another Lomer–Cottrell sessile dislocation $\frac{a}{6}[0\,1\,1]$, which cancels the one created by the leading partials. This sessile dislocation constricts the loop at the slip-plane intersection. Hence, the biplanar shear loop mechanism is applicable to the case where perfect dislocations decompose into partials. This is also clearly seen in the simulation of Fig. 8. The formation of sessile dislocations was successfully observed (molecular dynamics and quasi-continuum computational approaches) by Marian et al. [14,15] and is confirmed here, although there are differences in the details of the reaction.

5. Void growth kinetics

The Cocks–Ashby [44,45] model for void growth is, *strictu sensu*, only applicable to creep; the mechanisms of matter transfer are not dislocations but flow of vacancies along boundaries, surfaces or dislocations (the latter is the power-law creep, vacancies promoting the climb of dislocation segments). However, its form is such that it can be used for an ideally plastic material with strain rate sensitivity. The constitutive equation for power-law creep is

$$\dot{\varepsilon}_{ss} = \dot{\varepsilon}_0 \left(\frac{\sigma_e}{\sigma_0}\right)^n \tag{31}$$

where $\dot{\varepsilon}_{ss}$ is the equivalent strain rate, σ_e is the equivalent stress, and $\dot{\varepsilon}_0, \sigma_0$ and n are parameters. n is called the "power-law creep" exponent and is the inverse of the strain rate sensitivity. Cocks and Ashby [44,45] applied continuity

conditions to it in the presence of void and obtained the following equation for the evolution of damage, D

$$\frac{dD}{dt} = \beta \dot{\varepsilon}_0 \left[\frac{1}{(1-D)^n} - (1-D) \right] \left(\frac{\sigma_e}{\sigma_0} \right)^n \tag{32}$$

This constitutive equation was implemented by Bammann et al. [46] into finite element method codes to predict the failure of metals. The evolution of damage predicted by Cocks and Ashby [44,45] is dependent on the parameter *n*. In creep, it has a value between 1 and 10 (with $n = 5$ being the most quoted value), but in defining the strain rate sensitivity of plastic flow, the value of $(1/n)$ is much lower, on the order of 0.01, corresponding to $n = 100$. Integration of Eq. (32) yields the closed form solution

$$\ln |(1-D)^{n+1} - 1| - \ln |(1-D_0)^{n+1} - 1| = (n+1) \dot{\varepsilon} \beta t \tag{33}$$

The damage evolution in the MD calculations was estimated by considering the radius increase as a function of time. The initial damage D_0 was evaluated for a void radius $r = 2$ nm that gave an initial damage level $D_0 = 0.004$. Fig. 15a shows the evolution of damage for three crystal-line orientations: [001], [110] and [111]. The computation was carried out for a longer time for [001]; nevertheless, the results from the three orientations are compatible. The predictions of the Cocks–Ashby model are shown in the same plot and good agreement is obtained, the shape of the curves being similar. A significant difference is that there is an incubation time of 400 ps for the MD computations. This is the result of the time required to nucleate a dislocation (shear) loop. The match with Cocks–Ashby is best for a value of $n = 30$. This corresponds to a strain rate sensitivity of 0.033. This value is somewhat higher than the strain rate sensitivity often used for Ni at lower strain rates: 0.01. The higher strain rate sensitivity can be justified by the exceedingly high strain rate used in the present MD simulations: 10^8 s^{-1}. The Cocks–Ashby prediction can be easily extended to larger damages and this is shown in Fig. 15b for the values of *n* used in Fig. 15a. There is a gradual increase in the rate until $D = 0.2$. Beyond this value, damage proceeds essentially instantly.

6. Density of geometrically necessary dislocations

It is possible to estimate the total dislocation length around the expanding void using Ashby's [20–22] concept of geometrically necessary dislocations. This can be done in an approximate manner, by assuming that the dislocation loops transport matter outside.

The length of circumnavigating loop (each composed of six initial loops whose ends react) at an angle of 45° with the surface is:

$$\triangle L = 2 \left(\frac{2\pi r}{\sqrt{2}} \right) k + 6(kr - r) \tag{34}$$

where *k* is the extension ratio of the loop from its original value $(k = R/r)$. The distance that the dislocations travel outwards determines the radius *R* of the work-hardened layer (Fig. 16). The two terms represent the circular loop and six radii resulting from the reactions of loops extremities. The formation of two loops expands the void by a volume $\triangle V$ (Fig. 16)

$$\triangle V \simeq 2\sqrt{2}\pi r^2 b \tag{35}$$

The corresponding average increase in void radius, $\triangle r$, ignoring the distortion and other effects, is

$$\triangle r = (\triangle V)^{\frac{1}{3}} = \left(2\sqrt{2}\pi r^2 b \right)^{\frac{1}{3}} \tag{36}$$

The ratio of Eqs. (34) and (36) gives

$$\frac{dL}{dr} = \frac{\left[\frac{4\pi k}{\sqrt{2}} + 6(k-1) \right] r}{\left(2\sqrt{2}\pi r^2 b \right)^{\frac{1}{3}}} \tag{37}$$

Integrating

$$L = \frac{\left[\frac{4\pi k}{\sqrt{2}} + 6(k-1) \right]}{\left(2\sqrt{2}\pi b \right)^{\frac{1}{3}}} \int_{r_0}^{r_f} r^{\frac{1}{3}} dr \tag{38}$$
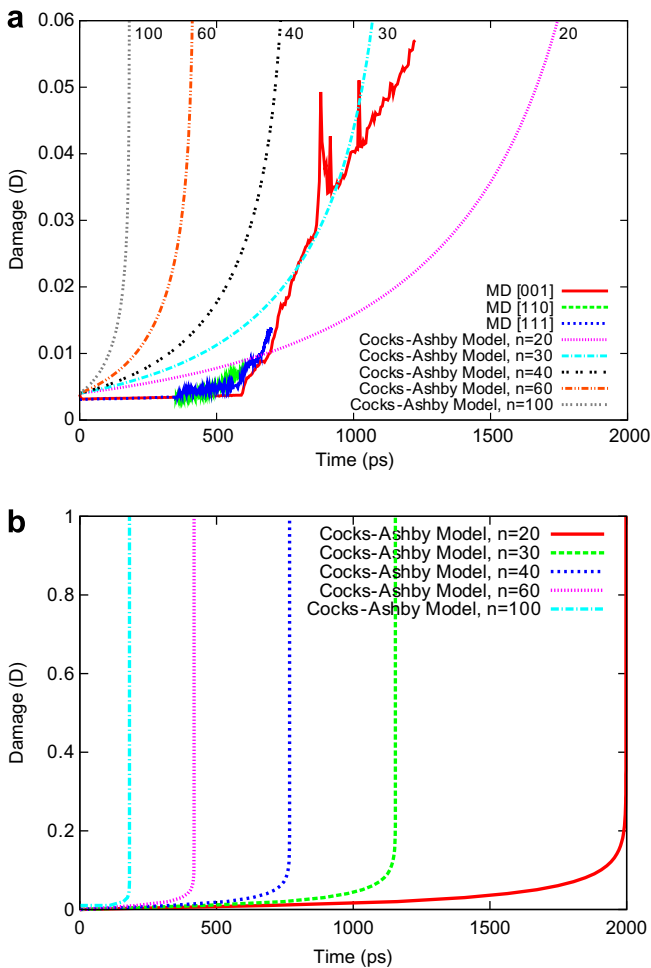

Fig. 15. Damage vs. time: (a) comparison of MD simulations and Cocks–Ashby equation and (b) predictions from Cocks–Ashby equation (*n* is exponent in power-law constitutive equation).
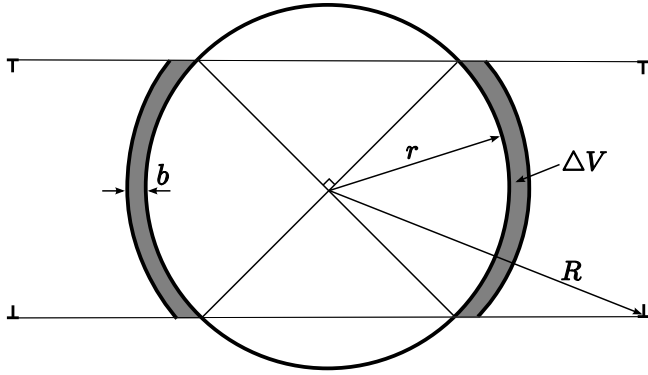
Fig. 16. Volume increment generated in void by the expansion of two shear loop rings.

If we make $r_0 = 0$

$$L = \frac{3\left[\frac{4\pi k}{\sqrt{2}} + 6(k-1)\right]}{4(2\sqrt{2}\pi b)^{\frac{1}{3}}} r^{\frac{4}{3}} \qquad (39)$$

The work-hardened volume is equal to

$$V_{\mathrm{wh}} = \frac{4}{3}\pi R^3 - \frac{4}{3}\pi r^3 = \frac{4}{3}\pi(k^3 - 1)r^3 \qquad (40)$$

The dislocation density is defined as

$$\rho = \frac{L}{V_{\mathrm{wh}}} = \frac{9\left[\frac{4\pi k}{\sqrt{2}} + 6(k-1)\right]}{16(2\sqrt{2}\pi b)^{\frac{1}{3}}\pi(k^3-1)} r^{-\frac{5}{3}} = F(k)r^{-\frac{5}{3}} \qquad (41)$$

The densities are plotted for values of k varying from 4 to 20 in Fig. 17. These values are consistent with dislocation densities in highly work-hardened metals. It is evident that k has to be larger for smaller voids, consistent with the mean free path of dislocations. As the void expands, the dislocation density can be accommodated with relatively a smaller work-hardened region. The prediction from Eq. 41 applies only to the geometrically necessary dislocations
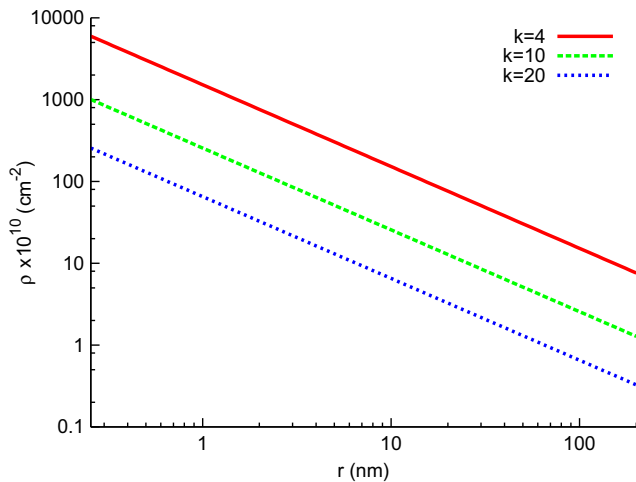

Fig. 17. Calculated density of geometrically necessary dislocations as a function of the ratio $k = \frac{R}{r}$.

and does not incorporate dislocation interaction effects that contribute to the statistically stored dislocation density.

7. Conclusions

1. Atomistic calculations combined with dislocation analysis reveal the detailed mechanism of void expansion in metals at strain rates in which diffusion does not play a role.
2. The nucleation is favored at slip planes that make an angle of 45° with the void surface, thus maximizing the shear stresses. This plane is translated outwards as the void grows, enabling the successive nucleation of loops.
3. Voids grow by the sequential nucleation, growth and expansion of loops from the void surface. The shear loop postulated by Lubarda et al. [8] is analyzed in greater detail for a two-dimensional configuration.
4. The expansion of shear loops on the six $\langle 110 \rangle$ directions is analyzed and the dislocation (both perfect and partial) reactions are calculated.
5. The atomistic calculations, carried out using the LAMMPS code using the embedded atom method with a Mishin [30] potential, show the partial dislocations and stacking faults after appropriate filtering. The shear loops emanating from the void surface can be observed, and a new mechanism of dislocation interaction was revealed: shear loops in intersecting $\{111\}$ planes react and there is no trailing stationary dislocation. In this biplanar loop mechanism, the expansion of the dislocation is easier than in the monoplanar mechanism of Lubarda et al. [8].
6. The effect of void size on the stress required for dislocation emission (onset of growth) is calculated by both MD and analytical means. This stress drops significantly in the void radius range investigated (0.5–4 nm). In contrast, the Gurson [2] prediction for the flow stress of a material containing voids is independent of the radius and is more consistent with larger voids.
7. The relationship between the stress required for void expansion and void size resembles closely the equation for the stress to bow a dislocation into a semi-circle, by equating the void and dislocation radii. This is consistent with MD results showing void expansion by shear loop formation.
8. The dislocation density around an expanding void is calculated based on Ashby's [20–22] concept of geometrically necessary dislocations. The densities obtained are consistent with those of highly work-hardened metals ($10^{11} - 10^{13}$ cm^{-2}).
9. The fundamental reason for the stress dependence of void growth stress expressed in Fig. 3 might also be connected to the discovery made by Horstemeyer et al. [25]. As mentioned in Section 1, they found a similar scale dependent yield behavior in specimens subjected to simple shear. Although this phenomenon has been earlier

attributed to strain gradient effects, Horstemeyer et al. [25] concluded that the reason for the scale dependence is altogether different. It is a matter of dislocation source availability, which becomes more and more restricted as the scale is decreased. As the void size is decreased beyond a certain threshold, the availability of maximum Schmid factor planes making 45° with the void surface and directions decreases. Thus, the stress required to generate the dislocation loop increases.

References

[1] McClintock FA, Argon AS, Backer S, Orowan E. Mechanical behavior of materials. Reading, MA: Addison-Wesley; 1966.
[2] Gurson AL. J Eng Mater Tech 1977;99:2.
[3] Needleman A, Tvergaard V. J Mech Phys Solids 1984;32:461.
[4] Tvergaard V, Needleman A. Acta Mater 1984;32:157.
[5] Potirniche GP, Hearndon JL, Horstemeyer MF, Ling XW. Int J Plasticity 2006;22:921.
[6] Cuitiño AM, Ortiz M. Acta Mater 1996;44:863.
[7] Stevens AL, Davison L, Warren WE. J Appl Phys 1972;43:4922.
[8] Lubarda VA, Schneider MS, Kalantar DH, Remington BA, Meyers MA. Acta Mater 2004;53:1397.
[9] Raj R, Ashby MF. Acta Metall 1975;23:653.
[10] Rudd RE, Belak JF. Comp Mater Sci 2002;24:148.
[11] Seppälä ET, Belak J, Rudd RE. Phys Rev B 2004;69:1.
[12] Seppälä ET, Belak J, Rudd RE. Phys Rev Lett 2004;93:1.
[13] Seppälä ET, Belak J, Rudd RE. Phys Rev B 2005;71:1.
[14] Marian J, Knap J, Ortiz M. Phys Rev Lett 2004;93:1.
[15] Marian J, Knap J, Ortiz M. Acta Mater 2005;53:2893.
[16] Dávila LP, Erhart P, Bringa EM, Meyers MA, Lubarda VA, Schneider MS, et al. Appl Phys Lett 2005;86:161902.
[17] Srinivasan SG, Baskes MI, Wagner GJ. J Mater Sci 2006;41:7838.
[18] Ahn DC, Sofronis P, Kumar M, Belak J, Minich R. J Appl Phys 2007;101.
[19] Potirniche GP, Horstemeyer MF, Wagner GJ, Gullett PM. Int J Plasticity 2006;22:257.
[20] Ashby MF. Phil Mag 1969;19:757.
[21] Ashby MF. Phil Mag 1969;20:1009.
[22] Ashby MF. Phil Mag 1970;21:399.
[23] Seitz F. Phys Rev 1950;79:723.
[24] Brown LM. Phil Mag 1970;21:329.
[25] Horstemeyer MF, Baskes MI, Plimpton SJ. Acta Mater 2001;49:4363.
[26] Meyers MA, Aimone CT. Prog Mater Sci 1983;28:1.
[27] Christy S, Pak Hr, Meyers MA. Metallurgical applications of shock wave and high-strain-rate phenomena. New York: Marcel Dekker; 1986.
[28] Plimpton SJ. J Comp Phys 1995;117:1.
[29] Daw MS, Baskes MI. Phys Rev B 1984;29:6443.
[30] Mishin Y, Mehl MJ, Papaconstantopoulos DA, Voter AF, Kress JD. Phys Rev B 2001;63:224106-1.
[31] Kelchner CL, Plimpton SJ, Hamilton JC. Phys Rev B 1998;58:11085.
[32] Aifantis EC. Int J Plasticity 1987;3:211.
[33] Fleck NA, Hutchinson JW. J Mech Phys Sol 1993;41:1825.
[34] Fleck NA, Muller GM, Ashby MF, Hutchinson JW. Acta Metall 1994;42:475.
[35] Gao H, Huang JY, Nix WD, Hutchinson JW. J Mech Phys Sol 1999;47:1239.
[36] Huang JY, Gao H, Nix WD, Hutchinson JW. J Mech Phys Sol 2000;48:99.
[37] Fu HH, Benson DJ, Meyers MA. Acta Mater 2001;49:2567.
[38] Fu HH, Benson DJ, Meyers MA. Acta Mater 2004;52:4413.
[39] Wen J, Huang Y, Hwang KC, Liu C, Li M. Int J Plasticity 2005;21:381.
[40] Hull D, Bacon DJ. Introduction to dislocations. 4th ed. Oxford: Butterworth-Heinemann; 2001.
[41] Van Swygenhoven H, Derlet PM, Frøset AG. Nature 2004;3:399.
[42] Cleri F, Rosato V. Phys Rev B 1993;48:22.
[43] Schiøtz J, Jacobsen KW. Science 2003;301:1357.
[44] Cocks ACF, Ashby MF. J Metal Sci 1980;14(8):395.
[45] Cocks ACF, Ashby MF. Prog Mater Sci 1982;27:189.
[46] Bammann DJ, Chiesa ML, Horstemeyer MF, Weingarten LI. In: Wierzbicki T, Jones N, editors. Failure in ductile materials using finite element methods, structural crushworthiness and failure. Elsevier Applied Science; 1993.